Defects production and annealing in self-implanted Si

G. Bai and M.-A. Nicolet
California Institute of Technology, Pasadena, California 91125

(Received 12 February 1991; accepted for publication 4 April 1991)

230-keV ^{28}Si ions were implantated into Si(100) at room temperature with doses from 10^{14} to $10^{15}/cm^2$. The samples were analyzed by x-ray double crystal diffractometry and 2-MeV ^4He ion channeling spectrometry. The implanted layer has a parallel lattice spacing equal to that of the unimplanted substrate. The perpendicular lattice spacing is larger than that of the unimplanted substrate and is proportional to the defect concentration extracted from the channeling measurement. Both the perpendicular lattice spacing and the defect concentration increase nonlinearly with ion dose. The defect concentration initially increases slowly with dose until a critical value ($\sim 15\%$, at $4\times10^{14}/cm^2$), then rises rapidly, and finally a continuous amorphous layer forms. The initial sluggish increase of the damage is due to the considerable recombination of point defects at room temperature. The rapid growth of the defect concentration is attributed to the reduction of the threshold energy for atomic displacement in a predamaged crystal. The amorphization is envisioned as a cooperative process initiated by a spontaneous collapse of heavily damaged crystalline regions. The annealing behavior of the damaged layer reveals various stages of defect recovery, indicating that the damage consists of a hierarchy of various defect structures of vacancy and interstitial aggregates.

I. INTRODUCTION

Radiation damage in semiconductors produced by energetic electrons or neutrons attracted much attention in the 1960s.[1] A great amount of information about the nature of simple defects and their annealing characteristics has been assembled with techniques such as electron paramagnetic resonance[2] and infrared optical absorption.[3] Since the 1970s, ion implantation and ion-solid interaction became the focus of investigation because of their technological importance.[4] Unlike electron-produced damage which consists of mainly isolated interstitials and vacancies, defects produced by ion implantation are complex.[5] Additional techniques such as channeling spectrometry,[6] transmission electron microscopy (TEM),[7] optical reflection spectroscopy,[8] and double crystal diffractometry,[9] have been used to reveal various aspects of the defect structure of ion-implanted semiconductors and Si in particular.[10] However, a detailed picture of the nature of defect production and their stability is still lacking. In recent years, ion implantation technology has found new applications in areas such as ion-beam induced epitaxial growth[11] and the synthesis of buried heterostructure.[12] The critical role of point defects produced by ion implantation in enhanced diffusion of dopants upon thermal annealing has been recognized.[13] An improved understanding of ion-induced defect production and annealing promises deepened insights in these phenomena.

Recognizing the important role that defects play, we undertook some quantitative analysis of damage produced by implantation of 230-keV ^{28}Si in a Si(100) crystal at room temperature. X-ray double crystal diffractometry and MeV ^4He channeling spectrometry were used to characterize the strain and the defect concentration. Some perspectives on the nature of defects are discussed in light of the experimental results.

II. EXPERIMENTAL RESULTS AND DISCUSSION

A. Sample preparation

The samples were prepared by implanting 230-keV ^{28}Si ions into 1-Ω cm n-type Si(100) wafers at room temperature in high vacuum ($\sim 10^{-7}$ Torr). The wafers were chemically cleaned before being loaded into the ion implanter. The surface normal was misoriented by 7° from the incidence line of the beam to avoid channeling. The beam current was limited to be low ($\sim 0.2\ \mu A/cm^2$) to minimize beam heating effects. The doses considered range from 10^{14} to $10^{15}/cm^2$.

B. Double crystal diffractometry

Double crystal diffractometry was used to monitor the strain (relative difference between the lattice constants of the implanted layer and the substrate). X-ray rocking curves of both symmetrical (400) and asymmetrical (311) diffractions were taken at room temperature in air 1 h after implantation and 6 months later. The strain profile as a function of depth is extracted by simulating the experimental rocking curve using dynamical x-ray diffraction (XRD) theory.[14] The parallel strain $\epsilon^{\parallel}$ of all samples considered here is zero within the experimental sensitivity ($\sim 10^{-4}$), meaning that the lateral lattice spacing in the implanted layer is constrained to be equal to that in the substrate. The perpendicular strain $\epsilon^{\perp}$ is positive and increases with dose, meaning that the perpendicular lattice spacing in the implanted layer is larger than that of the substrate and increases with the damage in the layer. The expansion of the lattice in the implanted layer implies that the strain contribution is dominated by the interstitial-like defects.[15] The magnitude of the perpendicular strain re-

 0021-8979/91/020649-07$03.00

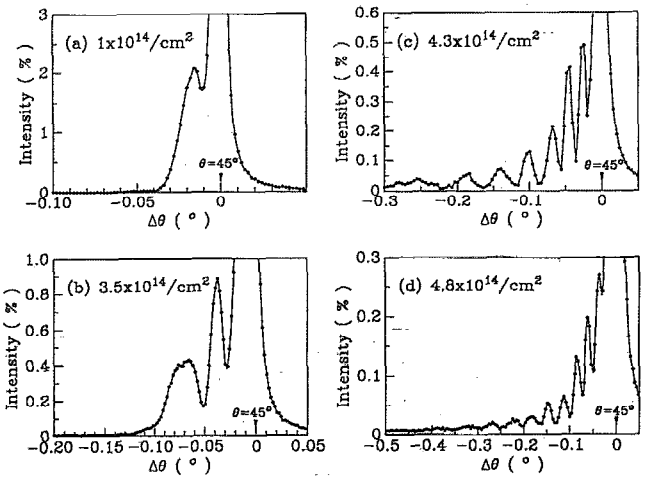

FIG. 1. Fe K_{α_1} x-ray rocking curves from the symmetrical (400) diffraction planes of Si(100) samples implanted with 230-keV ^{28}Si at room temperature to doses of (a) 1×, (b) 3.5×, (c) 4.3×, and (d) 4.8×10^{14}/cm^2.

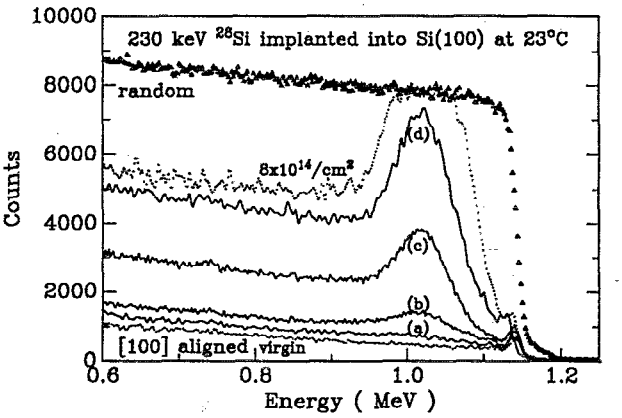

FIG. 3. 2-MeV ^{4}He backscattering and channeling spectra of the set of samples shown in Fig. 1. Also plotted are the channeling spectra of a virgin Si sample and one sample implanted with a Si dose of 8×10^{14}/cm^2 where a continuous amorphous layer forms.

laxes linearly with the logarithm of time at room temperature. The defects are almost stabilized at room temperature in <1 h after implantation. Subsequent to that, relaxation proceeds very slowly. We shall neglect this subsequent time dependence thereafter because it is minute ($\sim$0.02% in 6 months).

Figure 1 shows a set of selected x-ray rocking curves from symmetrical (400) diffraction. The x-ray diffraction peak intensity from the implanted layer decreases rapidly when the dose increases (notice ordinate scales). At the same time, the largest angular separation between the diffraction peaks of the implanted layer and the substrate increases. These facts mean that both the damage and the strain rise rapidly as the dose increases (notice abscissa scales). Figure 2 is a plot of the maximum perpendicular strain obtained from the strain profile versus implantation

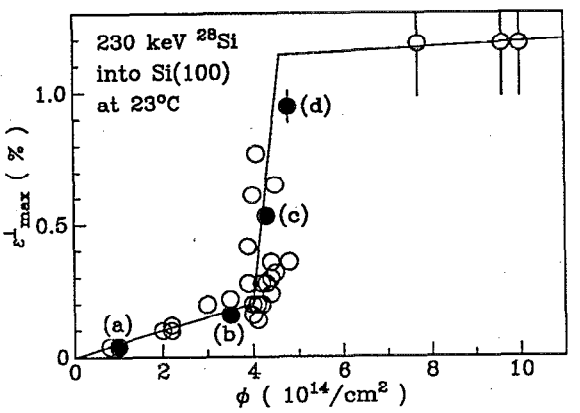

FIG. 2. The maximum perpendicular strain obtained from dynamic x-ray diffraction simulations of experimental rocking curves is plotted as a function of Si implantation dose. The solid line is to stress the trend. The filled circles correspond to the samples for which the x-ray rocking curves are plotted in Fig. 1.

dose. There exist three distinct regimes in this room-temperature implanted Si layer: (I) the strain builds up slowly until a critical dose of $\sim 4\times10^{14}$/ cm^2, (II) the strain then rises rapidly within a very narrow dose range and (III) finally saturates beyond a dose of $\sim 4.5\times10^{14}$/ cm^2. Dynamic x-ray diffraction simulation also gives an estimate of the static Debye–Waller factor $(\delta r)_{\rm rms}$ (the root-mean square of the atomic displacement from the lattice site). At any depth, the static displacement $(\delta r)_{\rm rms}$ is approximately proportional to the perpendicular strain. The maximum displacement is small in regime I ($\sim$0.01 nm), increases to $\sim$0.06 nm in regime II, and saturates at this value in regime III. One can obtain an "equivalent temperature," $T_{\rm eq}$, corresponding to the atomic displacement of $(\delta r)_{\rm rms}$, by using the Debye–Waller formula

$$(\delta r)^2_{\rm rms}=\frac{9\hbar^2 T_{\rm eq}}{Mk\Theta^2}, \tag{1}$$

where M is the mass of the silicon atom and $\Theta(=645$ K[16]) is the Debye temperature of crystalline Si. The maximum equivalent temperature thus obtained for the implanted Si layer is $\sim 0.2\,T_m$ ($T_m=1685$ K is the melting temperature) in the low damage regime (I), and reaches $\sim 4\,T_m$ in regime III. The very high equivalent temperature associated with regime III suggests that the heavily damaged state is far away from equilibrium and hence highly metastable.

C. Backscattering and channeling spectrometry

Backscattering and channeling spectrometry were used to measure the defect concentration in the implanted layer. Figure 3 shows 2-MeV ^{4}He [100] axial channeling spectra of selected samples. The defect concentrations were extracted from the channeling spectra according to the following model. The channeling yield χ_D of the damaged layer consists of two contributions: normal backscattering from the dechanneled fraction of an aligned incident beam,

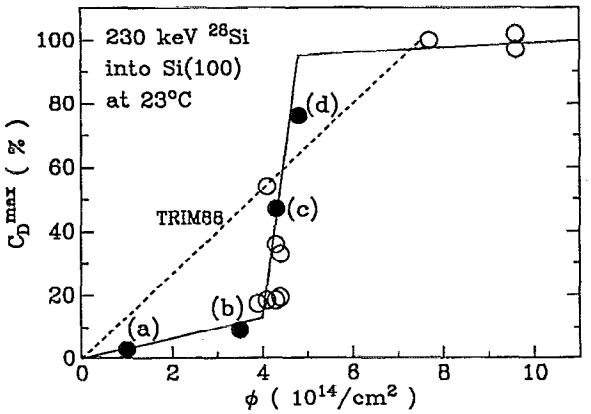

FIG. 4. The maximum defect concentration extracted from channeling spectra such as those of Fig. 3 as a function of the Si dose. The solid line is to highlight the trend. The filled circle corresponds to the samples shown in Fig. 3. The dashed line is the maximum value in the concentration profile of the Frenkel pair predicted by the TRIM 88 simulation code of 230-keV ^{28}Si implantation in an amorphous Si target.

χ_R, and direct backscattering of a channeled beam from the defect of concentration, c_D,[17]

$$\chi_D=\chi_R+(1-\chi_R)c_D. \tag{2}$$

The dechanneling of an aligned incident beam in the crystal equals

$$\chi_R=P_D+(1-P_D)\chi_V, \tag{3}$$

where P_D is the probability that a channeled incident ion is dechanneled by the defect and χ_V is the channeling yield of a virgin crystal. Combining Eqs. (2) and (3) gives

$$\gamma_D=c_D+(1-c_D)P_D, \tag{4}$$

where $\gamma_D\equiv(\chi_D-\chi_V/1-\chi_V)\in[0,1]$ is obtained directly from the channeling spectra of the virgin and the damaged crystals. In the single scattering approximation, one can define a dechanneling cross section σ_D,

$$\frac{dP_D}{dx}=n\sigma_D c_D, \tag{5}$$

where n is the atomic density of the crystal. From Eqs. (4) and (5), one finally obtains

$$\gamma_D(t)=c_D(t)+[1-c_D(t)]\int_0^t c_D(t')dt', \tag{6}$$

where $t\equiv n\sigma_D x$ is a dimensionless depth scale. Equation (6) is a nonlinear integral equation for the defect concentration c_D. Solving Eq. (6) numerically by adjusting the parameter σ_D to satisfy the boundary condition that P_D equals γ_D beyond the damaged layer (where $c_D=0$), the defect concentration profile $c_D(x)$ is obtained. The average best-fitted σ_D is $\sim 7\times10^{-19}$ cm^2, which is significantly smaller than the cross-sectional area of a channel. Figure 4 is a plot of the maximum defect concentration as a function of dose. Although derived from quite different experimental inputs, the dependence closely resembles that of strain-dose relationship and also exhibits the three distinct damage regimes with the same critical dose ($\sim 4\times10^{14}$/cm^2).

To elucidate what the amount of the measured damage means, we computed the maximum Frenkel pair concentrations produced by a 230-keV ^{28}Si implantation into an amorphous Si target at 0 K using the TRIM88 simulation program[18] (dashed line in Fig. 4). One sees that the measured damage in the low dose regime (I) is only $\sim$0.2 of that predicted. This means that the majority of initially created defects anneals out at room temperature. That result is consistent with the observation that single vacancies and interstitials are mobile at room temperature.[19] We thus conclude that the majority of initially created defects in regime I are in the form of simple Frenkel pairs which are mobile and readily recombine at room temperature. The measured stable defects are therefore di-vacancies, di-interstitials, and their clusters, formed during the migration of the point defects.[19]

In regime II, the damage increases with dose much faster ($\sim$8 times) than the production of Frenkel pairs calculated from TRIM88. This indicates that the defect production in the predamaged crystal is more efficient than that in a virgin crystal, suggesting that the newly produced defects can destabilize the crystal and cause the formation of disordered zones of increased size. Such a process produces about eight times more displacements than can be directly generated by nuclear collisions (see Fig. 4). In other words, in a predamaged crystal with a defect concentration $>15\%$, the effective threshold energy of atomic displacement is reduced from $\sim$15 eV[5] in the virgin crystal to $\sim$2 eV, which is approximately the formation energy of point defects in a solid by thermal activation.[5] Stated differently, the damage production depends on the interaction with existing defects beyond the critical defect concentration ($\sim$15%). The effect of dose is no more simply additive. Guided by our observation of accelerated growth of damage, we model the damage buildup phenomenologically by assuming that the production rate of stable defects is proportional to the concentration of existing defects. We also take into account the fact that the defects produced within already existing damage regions do not increase the defect concentration. Combining these two factors, we obtain the net rate of the production of the stable defects,

$$\frac{dc_D}{d\phi}=\frac{c_D+c_0}{\phi_0}\cdot(1-c_D), \tag{7}$$

where c_0 and ϕ_0 are fitting parameters. The solution is obtainable by direct integration and gives the growth of defect concentration as a function of dose. The best fit with experimental data gives $c_0\approx 2\times10^{-6}$ and $\phi_0\approx 3\times10^{13}$/ cm^2 (solid line in Fig. 5). The small value of c_0 reflects the difficulty in producing stable defects in a virgin crystal. This simple model fits the data reasonably well. Thompson *et al.*[20] also observed that the effective threshold energy for atomic displacement decreases as the energy density deposited in the nuclear collision increases. They attribute the enhancement to the thermal spike phenomenon. That phenomenon differs from what we observe in

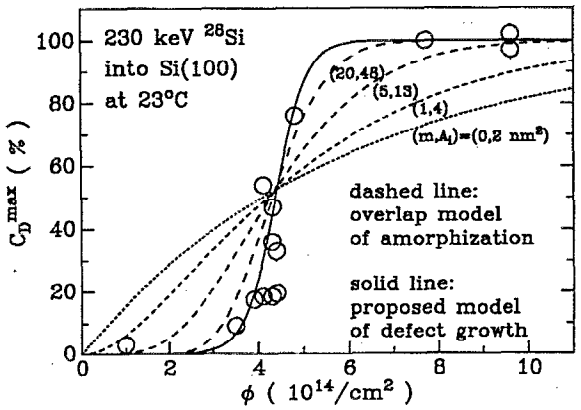

FIG. 5. The maximum defect concentration as a function of dose (○ of Fig. 4) compared with the defect concentration from the phenomenological model of the accelerated growth of damage in a predamaged crystal (solid line). The dashed lines are the fraction of the amorphous zones calculated from Gibbon's overlap model with various (m,A_i) parameters.

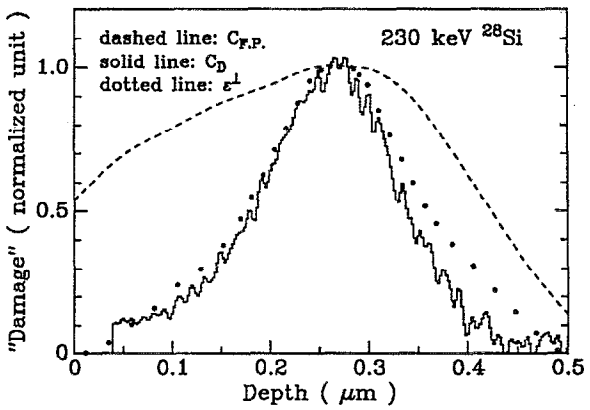

FIG. 6. The depth profile of the Frenkel pair concentration from TRIM 88 simulation (dashed line), the defect concentration from the channeling measurements of the sample (c) (solid line), and the perpendicular strain from dynamic diffraction model simulation of x-ray rocking curves (dotted line). The vertical scale is in arbitrary unit.

that the thermal spike also occurs in a virgin crystal. The enhancement seen here is caused by the existence of predamage, not the dense cascade produced by incident ion.

In regime III, a continuous amorphous layer is known to form at the maximum damage location when the yield for channeled beam incidence becomes the same as that for random beam incidence.[6] The dose for the onset of the formation of a continuous amorphous layer is $\sim 5\times 10^{14}$/cm^2 (see Fig. 4), which from TRIM88 simulation corresponds to a maximum energy density deposited in nuclear collision of $\sim 10^{24}$ eV/cm^3. This value agrees with the prediction of critical energy density criterion for amorphization ($\sim 10^{24}$ eV/cm^3).[5] Further implantation only causes the widening of the amorphous layer. To gain some insight in the mechanism of amorphization, we apply the Gibbons' overlap model[5] to fit the measured maximum defect concentration (dashed line in Fig. 5). Assuming that each incident ion creates a cylindrical zone of damage of cross section A_i and the formation of an amorphous region is caused by the m-tuple overlap of damage zones, the fraction of the amorphous regions f_A is given by[5]

$$f_A = 1 - \left(\sum_{j=0}^{m} \frac{(A_i\phi)^j}{j} \right) e^{-A_i\phi}. \tag{8}$$

Figure 5 shows several f_A curves with various parameters of (m, A_i). It is evident that the fitting improves as the m parameter increases (A_i increases correspondingly). This strongly suggests that the direct impact amorphization[21] by implanted ions does not occur in self-implanted Si at room temperature and that amorphous zones are formed due to the overlap of defected regions.[22] Furthermore, it is necessary to invoke very many overlaps ($m > 20$) to fit the rapid growth of damage. We thus hypothesize that amorphization may occur spontaneously as a result of collapses of heavily defected crystal.

D. Depth profile of "damage"

The depth profiles of the Frenkel pair concentration (c_{FP}, dashed line) obtained from TRIM88 simulations is compared with the defect concentration (c_D, solid line) extracted from channeling measurements of sample (c) in Fig. 6. To reveal the difference in the shapes of the damage-depth profiles, each profile is plotted by normalizing its peak value to unity. The measured profile is steeper than the calculated one, indicating that defects associated with smaller Frenkel pair concentration anneal out at room temperature, consistent with the above discussion. In particular, the measured defect concentration near the surface is more depleted compared to the simulated one, indicating that the surface is a very efficient sink for defects. Figure 6 also shows the depth profile of the perpendicular strain extracted from the simulation of x-ray rocking curves ($\epsilon^{\perp}$, dotted line), which closely follows that of the measured defect concentration c_D. The strain and the defect concentration are seen to be proportional to each other. Figure 7 shows the measured maximum strain in the implanted Si layer vs the measured maximum defect concentration. The two quantities are linearly related with a slope of ~ 0.013. This is constant over the entire range of strain and damage.

E. Relationship between strain and defect concentration

We apply continuum elasticity theory to estimate the order of magnitude of the coefficient relating the strain and the defect concentration in an implanted layer. To simplify mathematical expression, we treat the target as an elastically isotropic medium, although crystalline Si is anisotropic. Ion implantation produces defects in the implanted layer, which induces lattice expansion (or contraction), $\Delta a/a$. Assuming that the damaged layer is under biaxial stress imposed by the undamaged bulk substrate, the perpendicular and parallel elastic strains $e^{\perp}$ and $e^{\parallel}$, are then related by[23]

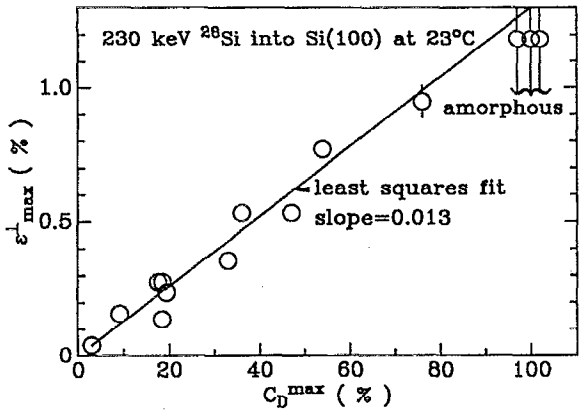

FIG. 7. The relationship between the maximum perpendicular strain and the maximum defect concentration.

$$\frac{e^{\perp}}{e^{\parallel}}=\frac{-2\nu}{1-\nu}, \tag{9}$$

where ν is Poisson's ratio. By definition, the elastic strain is related to the x-ray strain used in this paper,

$$\frac{e^{\perp}}{e^{\parallel}}\equiv\frac{\epsilon^{\perp}-\Delta a/a}{\epsilon^{\parallel}-\Delta a/a}. \tag{10}$$

From the above two equations, one derives the relationship between the lattice expansion $\Delta a/a$ and the strain,

$$\frac{\Delta a}{a}=\frac{1-\nu}{1+\nu}\epsilon^{\perp}+\frac{2\nu}{1+\nu}\epsilon^{\parallel}. \tag{11}$$

Substituting $\nu=0.28$ for Si and the measured value of $\epsilon^{\parallel}=0$ in the implanted layer into Eq. (11), one obtains

$$\frac{\Delta a}{a}=0.56\epsilon^{\perp}. \tag{12}$$

Figure 7 shows that the perpendicular strain $\epsilon^{\perp}$ in the implanted layer is proportional to the defect concentration c_D, we therefore obtain the relationship between the lattice expansion and the defect concentration,

$$\frac{\Delta a}{a}=0.007c_D. \tag{13}$$

Eshelby[24] showed that the lattice dilatation induced by point dilatation centers of concentration c and "strength" k equals

$$\frac{\Delta a}{a}=k\cdot c. \tag{14}$$

The strength of a dilatation center of radius R is given by[24,25]

$$k=\frac{4\pi(1-\nu)}{1+\nu}\cdot R^2\delta\cdot n, \tag{15}$$

where δ is the lattice displacement at R and n is the atomic density of a crystal [see Eqs. (8.6) and (8.7) of Ref. 24 and Eq. (2.24) of Ref. 25].

In face-centered-cubic (fcc) metals such as Cu, $k_v\sim-0.2$ for single vacancies and $k_i\sim 1.5$ for interstitials.[15,26] For a crystal containing equal number of single vacancies and interstitials, the strength becomes $k\sim 1.5-0.2=1.3$. This number is more than 100 times larger than the coefficient in Eq. (13). The smallness of the strength in Si could be due to the open structure of the diamond lattice compared to the closed-packed fcc lattice.[27] However, it is unlikely that this can explain the difference of more than two orders of magnitude.

Another explanation is that the defect in the room-temperature implanted Si is in the form of aggregates of vacancies and interstitials. To simplify the analysis, we will assume that the defect is in the form of vacancy and interstitial clusters containing an average of p lattice sites. We treat each cluster as an individual dilatation center of strength k_p. The lattice dilatation induced by the clusters of concentration c_p is therefore

$$\frac{\Delta a}{a}=k_p\cdot c_p, \tag{16}$$

according to Eq. (14). The strength k_p for the cluster can be obtained from Eq. (15),

$$k_p=\frac{4\pi(1-\nu)}{1+\nu}\cdot R_p^2\delta_p\cdot n. \tag{17}$$

The radius R_p of the cluster made of p lattice sites is related to the radius R_1 of one lattice site by

$$R_p=p^{1/3}R_1. \tag{18}$$

Furthermore, the displacement of a dilatation center is not sensitive to its size,[25] meaning that

$$\delta_p\approx\delta_1. \tag{19}$$

Applying the above two relations to Eq. (17), one obtains

$$k_p=p^{2/3}\left\{\frac{4\pi(1-\nu)}{1+\nu}\cdot R_1^2\delta_1\cdot n\right\}\equiv p^{2/3}\cdot k_1. \tag{20}$$

For a given defect concentration of c_D, the cluster concentration is

$$c_p=p^{-1}\cdot c_D. \tag{21}$$

Substituting Eqs. (20) and (21) into Eq. (16), one obtains the relationship between the lattice expansion and the defect concentration:

$$\frac{\Delta a}{a}=p^{-1/3}\cdot k_1\cdot c_D. \tag{22}$$

By substituting the typical value of $k_1\sim 1$ for a single vacancy interstitial pair in a fcc crystal into Eq. (22),[28] we have

$$\frac{\Delta a}{a}\approx p^{-1/3}\cdot c_D. \tag{23}$$

If $p\sim 3\times 10^6$, the coefficient in Eq. (23) becomes ~ 0.007, the same as that in Eq. (13). The diameter, D, of such a cluster is ~ 50 nm. This value is ten times larger than that observed by transmission electron microscopy

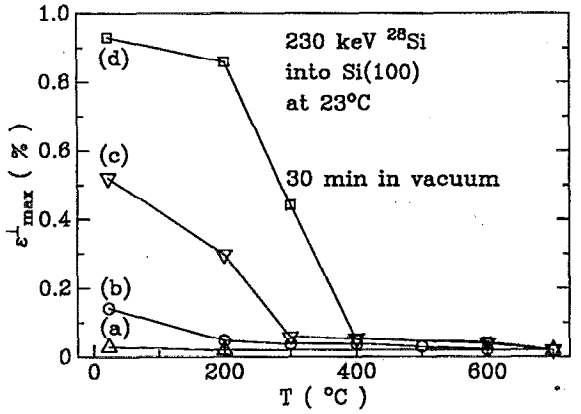

FIG. 8. The isochronal annealing characteristics of the perpendicular strain of Si implanted layers as a function of annealing temperature. All annealings were performed in a vacuum of $\sim 7 \times 10^{-7}$ Torr for a period of 30 min. The data shown are the four samples for which the x-ray rocking curves are plotted in Fig. 1 and the channeling spectra are plotted in Fig. 3.

(TEM).[29,30] By using the value from TEM, $D \sim 5$ nm, as the diameter of our cluster, and substituting the corresponding number of lattice site p into Eq. (22), we obtain

$$\frac{\Delta a}{a} \approx 0.07 \cdot k_1 \cdot c_D. \tag{24}$$

If the strength of a single vacancy interstitial pair k_1 in Si equals 0.1, the coefficient in Eq. (24) again becomes 0.007. This strength of point defects in Si is about ten times less than that in fcc metals.

This oversimplified model demonstrates that the observed smallness of the coefficient can be attributed to the combined effect of defect clustering and the small single vacancy interstitial strength. This is consistent with the fact that single vacancies and interstitials are mobile[19] at room temperature and Si has an open structure. The above analysis can be readily generalized to the more realistic defect structure where a distribution of different sizes of clusters exists.

F. Thermal annealing and damage recovery

In order to further reveal the nature of the defect in self-implanted Si, we conducted experiments to investigate the effect of thermal annealing on the strain in the implanted Si. It is known that single interstitials and vacancies anneal out at temperatures much less than room temperature,[19] di-interstitials anneal at 150° C,[31] di-vacancies anneal at ~100–250° C,[32] small damage clusters (<10 nm) anneal between 100 and 400° C,[33] and a continuous amorphous layer starts to regrow by solid phase epitaxy with appreciable rate at 550° C.[6] Isochronal annealings of the samples of Figs. 1 and 3 with different damage levels were performed in high vacuum (5×10^{-7} Torr) for 30 min at temperatures from 200 to 700° C. The parallel strain remains zero after annealing. The annealing behavior of the perpendicular strain is shown in Fig. 8. The temperature for significant recovery increases as the damage increases, indicating that different damage levels have different defect structures. Regime I with low damage [samples (a) and (b)] consists of relatively simple defects such as di-interstitials and di-vacancies. The intermediate damage regime (II) [samples (c) and (d)] contains more complex defects such as clusters or small disordered zones. As the damage increases further, a continuous amorphous layer forms due to the overlap of the damaged regions. This picture differs from Vook and Stein's,[34] where there are only two distinct annealing stages at ~ 250 and ~550° C, which they associated with the annealing of di-vacancies and epitaxial growth of amorphous layer, respectively. They accordingly proposed that amorphization is controlled by di-vacancy annealing.[34,35] Our results are based on data taken with fine increments of the dose near the amorphization threshold (Figs. 2 and 4) and reveal a complex defect hierarchy.

III. CONCLUSIONS

In light of the above experimental results and discussion, we propose the following model for the damage buildup and amorphization of self-implanted Si at room temperature. Initially, the majority of defects produced by incident ions in a virgin crystal are Frenkel pairs, which are mobile at room temperature. The migration of these interstitials and vacancies results in recombination and clustering to form stable defects such as di-interstitials and di-vacancies. Only a small fraction of initially created defects remain at room temperature. They generate perpendicular strain. As the damage rises to the critical value (~15%), a large amount of energy is stored in the damaged layer. Additionally created defects cause the collapse of the damaged region into large disordered zones. This mechanism produces more damage than that generated directly by nuclear displacements, giving rise to an enhanced production of damage and strain. The larger the damage, the more complex the defect structure becomes. Amorphization occurs spontaneously as a cooperative process due to the overlap of heavily defected crystalline regions. The damage production reported here for room-temperature implantation of Si into Si differs from that similarly produced in GaAs in two respects: (1) The damage relaxation at room temperature in irradiated Si is minute, while in irradiated GaAs it is significant.[36] (2) After the initial linear rise with the Si dose, the increase of the damage production accelerates in Si, but decelerates in GaAs.[37] This divergent behavior of Si and GaAs is noteworthy of further investigation.

ACKNOWLEDGMENTS

The authors thank Dr. T. Vreeland, Jr. for constructive comments, Dr. W. L. Johnson for helpful discussions, and Mr. C. J. Tsai for providing the rocking curve fitting program. This work is supported in part by the Semiconductor Research Corporation under Contract No. 100-SJ-89 and by the National Science Foundation under Grant No. DMR-8811795. The authors gratefully acknowledge this support.

[1] *Radiation Effects in Semiconductors*, edited by F. L. Vook (Plenum, New York, 1968).
[2] G. D. Watkins, J. Phys. Soc. Jpn. **18**, Suppl. II, 22 (1963).
[3] L. J. Cheng, J. C. Corelli, J. W. Corbett, and G. D. Watkins, Phys. Rev. **152**, 761 (1966).
[4] *Proc. Ist Int. Conf. on Ion Implantation*, edited by L. Chadderton and F. Eisen (Gordon and Breach, New York, 1971).
[5] J. F. Gibbons, Proc. IEEE **60**, 1062 (1972).
[6] J. W. Mayer, L. Eriksson, S. T. Picraux, and J. A. Davis, Can. J. Phys. **46**, 663 (1968).
[7] M. L. Swanson, J. R. Parsons, and C. W. Hoelke, *Radiation Effects in Semiconductors*, edited by J. W. Corbett and G. D. Watkins (Gordon and Breach, New York, 1971), p. 359.
[8] S. Kurtin, G. A. Shifrin, and T. C. McGill, Appl. Phys. Lett. **14**, 223 (1969).
[9] V. S. Speriosu, B. M. Paine, M. -A. Nicolet, and H. L. Glass, Appl. Phys. Lett. **40**, 604 (1982).
[10] E. Glaser, G. Götz, N. Sobolev, and W. Wesch, Phys. Status Solidi A **69**, 603 (1982).
[11] J. S. Williams, R. G. Elliman, W. L. Brown, and T. E. Seidel, Phys. Rev. Lett. **55**, 1482 (1985).
[12] A. E. White, K. T. Short, R. C. Dynes, J. P. Garno, and J. M. Gibson, Appl. Phys. Lett. **50**, 95 (1987).
[13] P. A. Packan and J. D. Plummer, Appl. Phys. Lett. **56**, 1787 (1990).
[14] C. R. Wie, T. A. Tombrello, and T. Vreeland, Jr., J. Appl. Phys. **59**, 3743 (1986).
[15] L. Tewordt, Phys. Rev. **109**, 61 (1958).
[16] C. Kittel, *Introduction to Solid State Physics*, 5th ed. (Wiley, New York, 1976), p. 126.
[17] E. Bogh, Can. J. Phys. **46**, 653 (1968).
[18] J. P. Biersack and L. G. Haggmark, Nucl. Instrum. Methods **174**, 257 (1980).
[19] J. W. Corbett, J. P. Karins, and T. Y. Tan, Nucl. Instrum. Methods **182/183**, 457 (1981).
[20] D. A. Thompson and R. S. Walker, Nucl. Instrum. Methods **132**, 281 (1976).
[21] F. F. Morehead, Jr. and B. L. Crowder, Radiat. Effects **6**, 27 (1970).
[22] J. R. Dennis and E. B. Hale, J. Appl. Phys. **49**, 1119 (1978).
[23] See, for example, L. D. Landau and E. M. Lifshitz, *Theory of Elasticity* (Pergamon, Oxford, 1986), Chap. I.
[24] J. D. Eshelby, *Solid State Physics*, edited by F. Seitz and D. Turnbull (Academic, New York, 1956), p. 79.
[25] M. W. Thompson, *Defects and Radiation Damage in Metals* (Cambridge University, Cambridge, 1969), p. 16.
[26] H. G. Haubold and D. Martinsen, J. Nucl. Mater. **69/70**, 644 (1978).
[27] F. L. Vook, Phys. Rev. **125**, 855 (1962).
[28] R. O. Simmons and R. W. Balluffi, J. Appl. Phys. **30**, 1249 (1959).
[29] D. J. Mazey, R. S. Nelson, and R. S. Barnes, Philos. Mag. **17**, 1145 (1968).
[30] M. O. Ruault, J. Chaumont, and H. Bernas, Nucl. Instrum. Methods **209/210**, 351 (1983).
[31] W. Jung and H. S. Newell, Phys. Rev. **132**, 648 (1963).
[32] H. J. Stein, F. L. Vook, and J. A. Borders, Appl. Phys. Lett. **14**, 328 (1969).
[33] L. M. Howe, M. H. Rainville, H. K. Haugen, and D. A. Thompson, Nucl. Instrum. Methods **170**, 419 (1980).
[34] F. L. Vook and H. J. Stein, Radiat. Effects **2**, 23 (1969).
[35] O. W. Holland, S. J. Pennycook, and G. L. Albert, Appl. Phys. Lett. **55**, 2503 (1989).
[36] G. Bai, D. N. Jamieson, M. -A. Nicolet, and T. Vreeland, Jr., Mater. Res. Soc. Symp. Proc. **93**, 67 (1987).
[37] B. M. Paine and V. S. Speriosu, J. Appl. Phys. **62**, 1704 (1987).